Update on Quadruple Suspension Design for Advanced LIGO

S.M. Aston[1,8], M.A. Barton[2], A. S. Bell[3], N. Beveridge[3], B. Bland[2], A.J. Brummitt[4], G. Cagnoli[3], C.A. Cantley[3], L. Carbone[1], A.V. Cumming[3], L. Cunningham[3], R.M. Cutler[1], R.J.S. Greenhalgh[4], G.D. Hammond[3], K. Haughian[3], T.M. Hayler[4], A. Heptonstall[5], J. Heefner[5,†], D. Hoyland[1], J. Hough[3], R. Jones[3], J.S. Kissel[9], R. Kumar[3], N.A. Lockerbie[6], D. Lodhia[1], I.W. Martin[3], P.G. Murray[3], J. O'Dell[4], M.V. Plissi[3], S. Reid[7], J. Romie[8], N.A. Robertson[5,3,*], S. Rowan[3], B. Shapiro[9], C.C. Speake[1], K.A. Strain[3], K.V. Tokmakov[6], C. Torrie[5,3], A.A. van Veggel[3], A. Vecchio[1], I. Wilmut[4]

1 School of Physics and Astronomy, University of Birmingham, Edgbaston, Birmingham, B15 2TT, UK
2 LIGO Hanford Observatory, PO Box 159, Richland, WA 99352, USA
3 SUPA, Institute for Gravitational Research, School of Physics and Astronomy, University of Glasgow, Glasgow, G12 8QQ, UK
4 Engineering Department, Rutherford Appleton Laboratory, Didcot, Oxon, OX11 0QX, UK
5 LIGO Laboratory, California Institute of Technology, MS 100-36, Pasadena CA 91125, USA
6 SUPA, Department of Physics, University of Strathclyde, John Anderson Building, 107 Rottenrow, Glasgow, G4 0NG, UK
7 SUPA, Thin Film Centre, University of the West of Scotland, High Street, Paisley, PA1 2BE, UK
8 LIGO Livingston Observatory, P.O. Box 940, Livingston, LA 70754, USA
9 LIGO Laboratory, Massachusetts Institute of Technology, 185 Albany St, Cambridge MA 02139, USA

Abstract

We describe the design of the suspension systems for the major optics for Advanced LIGO, the upgrade to LIGO - the Laser Interferometric Gravitational-Wave Observatory. The design is based on that used in GEO600 – the German/UK interferometric gravitational wave detector, with further development to meet the more stringent noise requirements for Advanced LIGO. The test mass suspensions consist of a four-stage or quadruple pendulum for enhanced seismic isolation. To minimize suspension thermal noise, the final stage consists of a silica mirror, 40 kg in mass, suspended from another silica mass by four silica fibres welded to silica ears attached to the sides of the masses using hydroxide-catalysis bonding. The design is chosen to achieve a displacement noise level for each of the seismic and thermal noise contributions of 10^{-19} m/√ Hz at 10 Hz, for each test mass. We discuss features of the design which has been developed as a result of experience with prototypes and associated investigations.

1. Introduction

The US Laser Interferometric Gravitational-Wave Observatory, LIGO, consists of three detectors, two at Hanford, Washington State and one at Livingston, Louisiana (Sigg et al. 2008). The detectors reached their initial design sensitivity in 2006 and were operated for several years to search for gravitational waves of astrophysical origin. No such detections have yet been made, a result which is not surprising given the likely strength of signals and the initial sensitivity. An increase in sensitivity is needed to reach a level where

† Deceased April 2012
* Corresponding author nroberts@ligo.caltech.edu

signals should be routinely detected. The Advanced LIGO project, aLIGO (Harry et al. 2010), is designed to increase the sensitivity of the LIGO detectors by approximately an order of magnitude and extend the working frequency band at the lower end from ~40 Hz down to ~10 Hz. To achieve these improvements in performance all the key hardware is being upgraded including the laser, the optics, the seismic isolation systems and the suspensions, as well as introducing signal recycling to tune the quantum noise performance. First astrophysical searches with aLIGO are expected in 2015.

Gravitational waves are ripples in the curvature of spacetime which propagate at the speed of light. A passing wave distorts spacetime and results in a relative displacement change between free, or inertial, test masses. An interferometer provides a convenient method for making measurements of such changes. The aLIGO detector topology comprises a Michelson interferometer with Fabry-Perot cavities (Harry et al. 2010) and incorporates four test masses in each detector, one at each end of each arm. These test masses are required to be suspended to act as inertial masses in the frequencies of interest and to provide isolation from seismic disturbances. The aLIGO suspension designs for the test masses are based on the design used for the test masses in GEO600, the German/UK gravitational waves project (Plissi et al. 1998, Plissi et al. 2000, Husman et al. 2000, Gossler 2004)). The aLIGO test mass suspension consists of a quadruple pendulum incorporating three stages of maraging steel blade springs for enhanced vertical isolation. To minimize the thermal noise associated with the pendulum modes of the suspension, the final stage consists of a silica mirror, 40 kg in mass, suspended from another silica mass by four silica fibres welded to silica ears which are attached to the sides of the mass using hydroxide-catalysis bonding (silicate bonding) (Gwo D-H 2001). The final stage is thus a monolithic fused silica suspension. Control signals to damp the low frequency modes are applied at the top mass, thus allowing for isolation of electronic noise associated with this control by the stages below. A second quadruple pendulum called the reaction chain is suspended adjacent to the main chain and is used for applying global control signals from a quiet platform to hold the interferometer close to a dark fringe. The design for the test mass suspensions is chosen to achieve a displacement noise level for each of the seismic noise and thermal noise contributions of 10^{-19} m/$\sqrt{}$ Hz at 10 Hz, for each test mass. Figure 1 shows a representation of the quadruple pendulum and its reaction chain. This paper represents an update to the publication in which the conceptual design for these suspensions was presented (Robertson et al. 2002). Since that time there have been several modifications to the design and lessons learnt from building and testing prototype suspensions. We are now assembling and testing the production items for aLIGO, with installation of the first suspensions into the detectors having started in late 2011. In the following sections we describe in detail the various aspects of the design and discuss features which have been developed as a result of experience with our prototypes and associated investigations.

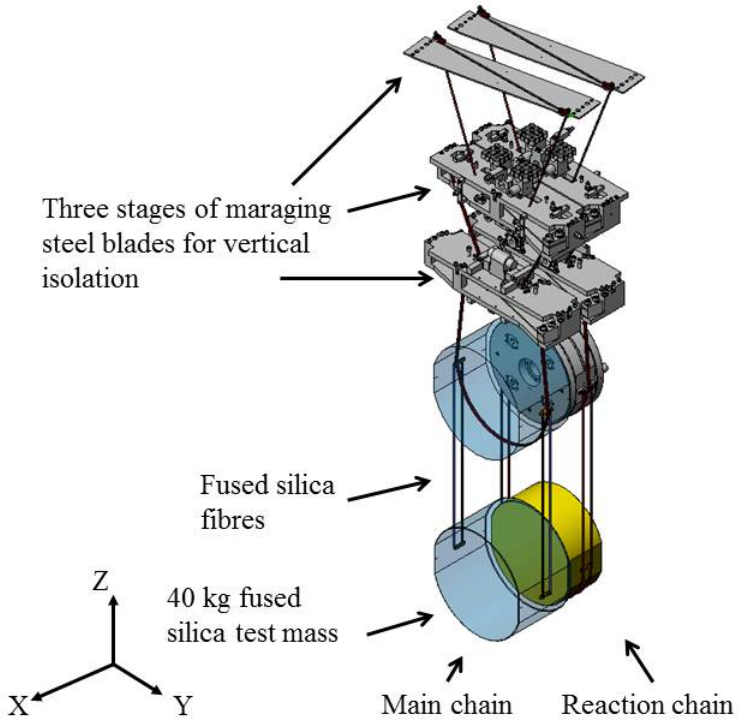

Figure 1. Drawing of quadruple pendulum with quadruple reaction pendulum hanging behind it. The coordinate system is also indicated.

2. Mechanical design

The overall mechanical design may be considered as having three elements: the suspended masses, the structure surrounding the chains, and the auxiliary components. Horizontal isolation is provided by the natural pendulum action; vertical isolation is provided in large part by soft blade springs which introduce significant vertical compliance. Figure 2 shows a drawing of the quadruple pendulum in its support structure with the reaction chain hanging behind it.

2.1 General requirements

Requirements for all of the suspension parts included vacuum compatibility which, given the target vacuum levels of approximately 10^{-9} Torr, meant that components had to be metal or ceramic in nearly all cases, and placed strict requirements on the design and manufacturing processes to avoid trapped volumes and ensure any contaminants could be cleaned off. Where the use of elastomers could not be avoided – in the earthquake stops and in the clamps used for electrical wiring - we used a custom fluoroelastomer.

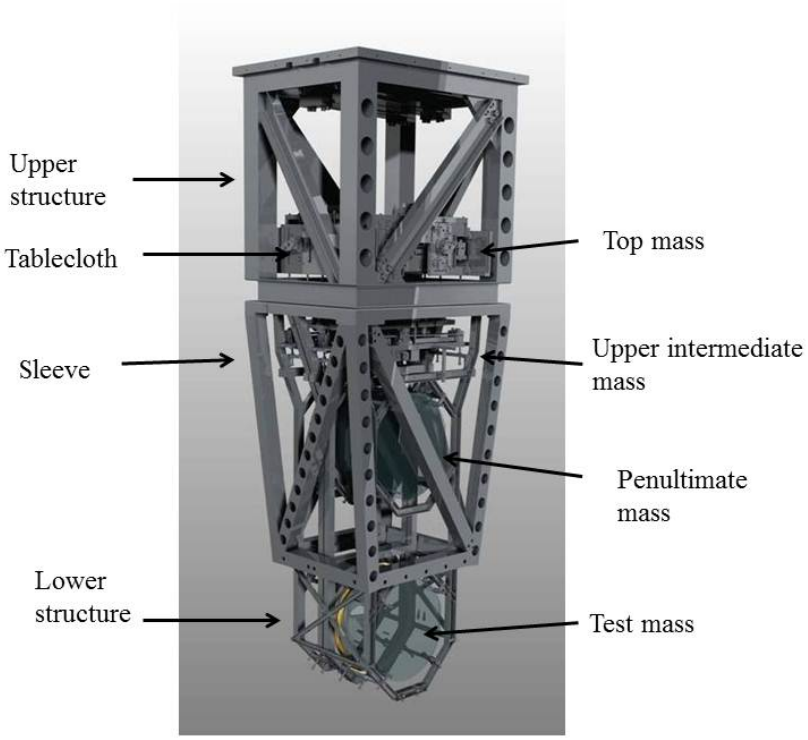

Figure 2. Drawing of quadruple pendulum and reaction pendulum with its surrounding support structure. Some key elements are labeled.

We aimed to maximize commonality of parts in order to reduce costs. At the same time we aimed for ease of assembly as far as reasonably practicable – for example we provided places where measurements could be readily made where adjustments are required, and minimized the number of different screw sizes. To reduce shedding, we included thread inserts in places where screws might need to be adjusted once the suspension is assembled (we also used thread inserts in places where extra strength is required such as for the bolts that clamp the roots of the blade springs). The use of inserts had a major practical disadvantage – they are hard to remove, and the parts cannot be cleaned with them in place. In all aspects of the design, we built as far as possible on the design heritage from the successful GEO suspensions. Overall, approximately 1,500 custom-made parts and 2,000 off-the-shelf components went into each of the suspensions. The chains were designed so that, if a decision were made later to switch to test masses of sapphire of the same mass and radius, it would be possible to move the chains closer together to allow for the thinner sapphire test mass.

2.2 The suspended masses

There are two chains of suspended masses – the so-called “main chain” and the “reaction chain” as shown in figure 1. The overall design of the two chains in terms of masses, blades, wire lengths and attachment points is very similar for ease of fabrication and damping control. In each chain there are four masses totaling approximately 120 kg, with the bottom two masses summing to 80 kg. The main chain has masses of approximately

20, 20, 40 and 40 kg respectively from top to bottom. For reasons discussed below, the reaction chains at either end of the Fabry-Perot cavities are different. For the chain at the end of the interferometer arms the masses are 20, 20, 54 and 26 kg whereas for the chain close to the beam splitter they are 20, 20, 60 and 20 kg The masses need to provide anchoring points for the wires and the blade springs, with suitably designed clamps which provide a sharp break-off point for the wire or blade, in order to minimize frequency upconversion from rubbing as the wire or blade flexes. A final requirement on the mass design was that there should be no low frequency internal vibration modes involving significant mass to disturb the control systems.

The masses are connected by silica fibres (between test mass and penultimate mass) or wires (all other cases). The top masses are suspended by two wires to minimise pitch transmission from the suspension point. In all other cases there are four wires so that both pitch and roll motions are coupled between masses. The wires were arranged to be non-vertical in order to suitably couple 22 of the 24 pendulum modes of the four-stage pendulum; this means that these 22 modes are observable at the top mass and can be damped there. See section 4 for more details on the damping. The highest two modes, which are the highest vertical and roll modes, and which involve extension of the silica fibers, are very weakly coupled to external forces and remain undamped.

The top mass in each chain consists of a stainless steel plate approximately 500 mm long by 150 mm wide by 15 mm thick, with features to allow attachment of the wires supporting it from above, the blade springs which provide support to the masses below, the magnetic flags which are acted on by the Optical Sensors/ElectroMagnetic actuator (OSEM) units, adjustable earthquake stops, and pitch adjusters. The OSEMs at this top stage are all mounted on the structure to apply active damping.

The upper intermediate mass in each chain is similar to the top mass, except that there are OSEMS on the upper intermediate reaction mass acting on the upper intermediate mass in the main chain to allow global control forces to be applied (discussed further in Section 4.3).

The penultimate mass is a cylinder with the rotational axis of symmetry aligned with the test mass. In the main chain it is made of silica, and in the reaction chain it is made of metal. There are no blade springs in the penultimate mass so that the penultimate and test masses can be connected by silica fibres (the so-called “monolithic stage”) to keep the thermal noise low. The penultimate mass in the main chain includes features to house the flags for the OSEMs, the OSEMs themselves being mounted on the penultimate reaction mass. As in the upper intermediate mass, these OSEMs are used for applying global control forces. The penultimate reaction mass includes features to give it the correct moments of inertia as well as mass.

The silica test mass is a circular cylinder of diameter 340 mm and thickness 200 mm with flats on the sides and a small wedge. The reaction mass adjacent to the test mass is also made of silica of diameter 340 mm. At the far ends of the interferometer arms, the main beam is reflected by the test mass, with a very small amount transmitted for alignment

purposes. At the inner ends, however, the main beam passes through both test and reaction masses. This reaction mass, known as the compensator plate, is used to compensate for the optical effects of the expansion of the test masses caused by heating from the laser beam (Fritschel et al. 2009). The compensator plate has a thickness of 100 mm, significantly thinner than the reaction mass for the end test masses (the end reaction mass) which has a thickness of 130 mm. Thus as the compensator plate hangs in the reaction chain there is a significant gap between it and the test mass of 20 mm. This was done to reduce damping caused by the residual gas in the gap (Cavalleri et al. 2009). At the end test mass chamber the gap is 5 mm. A lower pressure is expected to be achieved in those vacuum tanks, reducing the gas damping effect.

2.3 The structures

The principal requirements on the structures, in addition to the generic requirements mentioned above, are that they must be strong enough to support the masses in the case of an earthquake, and stiff enough to prevent excessive movement. Their internal modes must be high in order to avoid interference with the active control system of the seismic isolation platforms to which they are mounted. They provide anchoring points for the OSEMs used for active damping, the earthquake stops, and the ring heaters providing thermal compensation for the test masses (Fritschel et al. 2009), and guards for fibres. They must provide access for adjustments during and after assembly of the chains that fit within them, and they allow for fiducial scribe marks used during alignment of the interferometer.

In order to give the required combination of stiffness with accessibility we designed the structure in two parts. The upper structure, which is welded from hollow rectangular section for stiffness, incorporates the springs at the very top of the suspensions (the so-called “top stage”) and the top masses. The lower structure surrounds the upper intermediate, penultimate, and test masses, and has two layers. The inner layer consists of large machined parts bolted together to allow the detailed features required for interfacing to the suspended masses, with an outer “sleeve”, welded from hollow square section. All welding is full penetration for ultra-high vacuum compatibility. The upper structure also has a machined inner part, called the “tablecloth”, with fits closely around the top mass – part of the design heritage from the GEO suspension systems. See figure 2.

A significant amount of finite element modeling was done in order to maximize the natural frequency of the structures, with a target of 100 Hz for the first bending mode for a structure rigidly fixed at the base. We were not able to directly compare the finite element modeling with experimental results, because the structure is not in reality mounted on an infinitely stiff base like the model. The measured result in situ was approximately 75 Hz and this has proved to be acceptable with the use of some additional damping units attached to the structure to lower the quality factors of the first few structural resonances (Biscans S and Matichard F 2010).

2.4 The suspension wires

The wires are made of steel music wire, mostly straight, with a clamp at each end. The exceptions are the wires supporting the silica reaction mass and the silica penultimate mass where the wires take the form of “loops” running from the mass above, under the mass in question, and back to the mass above. The wire diameters were chosen to give a safety factor of approximately three over the breaking stress.

2.5 Blade springs

2.5.1 Overall form

The purpose of the blade springs is to provide vertical compliance in order to lower the vertical oscillation frequencies of the suspension chains. They draw on the heritage of the VIRGO and GEO suspensions (Braccini et al. 2000, Plissi et al. 2000). The form is a cantilever of constant thickness, tapering in width towards the tip. With a point load at the tip, this gives a uniform bending radius. The blades are made to a curved shape so that, when loaded, they are approximately flat. The material is a maraging steel which gives high strength (allowing the spring to be made soft) but with ductility for safety. Maraging steel also has the property that noise from dislocation movement under load is very low (Beccaria et al. 1998). The blades are made by grinding stock material to the correct thickness and then curling them between rollers to the right radius of curvature before final martensitic ageing to harden them. Extensive studies using analytical techniques and finite element analysis, were backed up with prototyping in order to be sure that the blades would have the desired stiffness and correct deflected shape under load. With a deflection of up to 300 mm, it is important that the blades have the right stiffness – a small error in stiffness would give large errors in deflected shape and make the suspension very difficult to align. In order to guard against corrosion and the possibility of stress-corrosion cracking, the blades were nickel plated after manufacture. Certain other effects needed to be allowed for in the design, as noted below.

2.5.2 Geometrical antispring effect

The wires attached to the tips of the springs are not vertical. To varying degrees they are angled towards the root of the blade, so the load on the tip has a longitudinal, as well as a vertical, component. A longitudinal load on a straight blade will have no effect on blade deflection. However, the blades are typically not straight in operation, so any longitudinal load will generate a bending moment at the tip (as shown in figure 3, fourth diagram). This moment will cause additional deflection of the blade, so the overall blade deflection is greater than would be the case were the wires vertical. This effect tends to soften the vertical compliance of the springs and make the vertical frequencies lower than would be seen without this effect. For example, the top springs are each loaded by 62 kg at an angle of 21 degrees, and show a reduction in vertical stiffness to 70% of the value they would have under purely vertical load.

2.5.3 Lateral compliance, wire stiffness, and breakoff points

In order to keep the natural frequencies low, the points at which masses are supported by the wire from the mass above, and the points at which the wires leave to go to the mass below, are set to be close to the plane of the centre of mass in the direction that provides stability. However, if these so-called breakoff points are on the wrong side of the centre

of mass plane, the mass will be unstable against tipping (pitching). Three effects make this part of the design non-trivial.

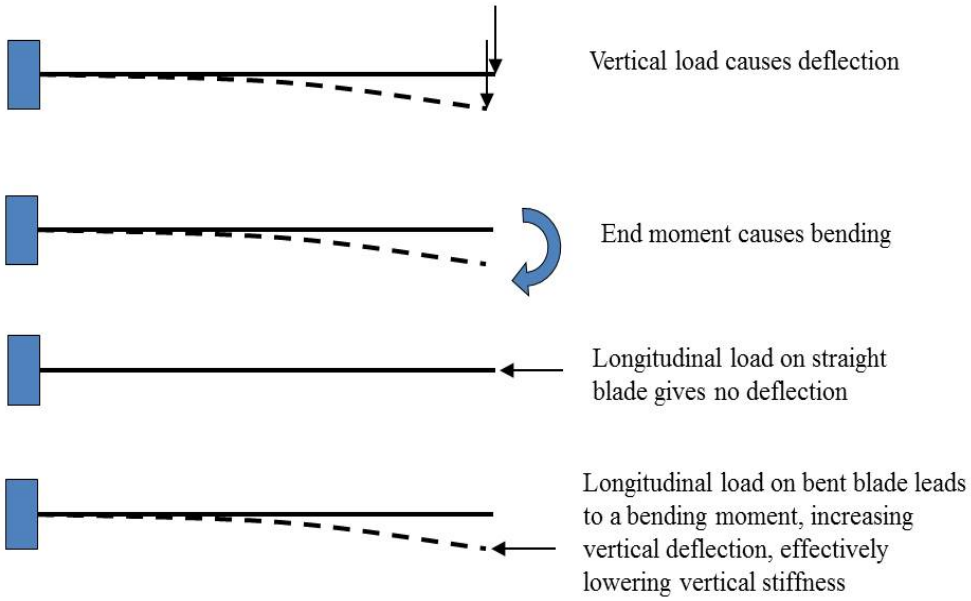

Figure 3. Illustration which shows how a longitudinal load can lower the vertical stiffness of a blade spring

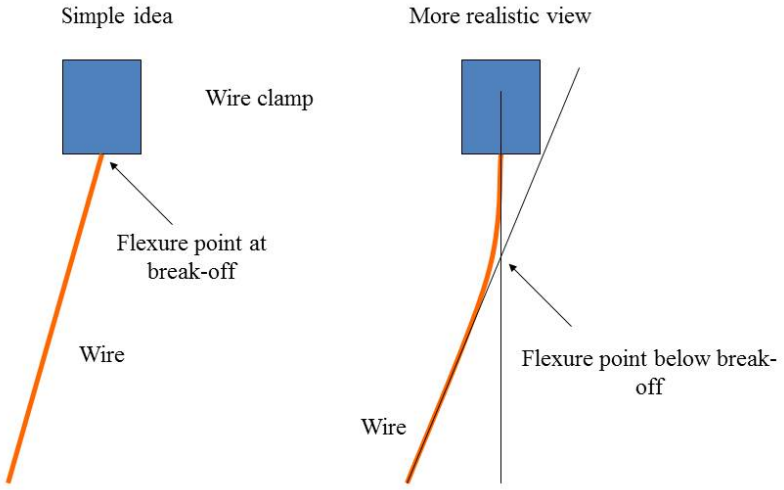

Figure 4. Illustration which shows how there is a flexure point at some distance from the break-off point

1. The deflection of the blades when loaded is of the order hundreds of mm, whereas the target offset from the centre of mass plane is of order 1 mm. Small errors in the blade deflection can give large errors in the offset.

2. The wires have a natural bending stiffness which leads to a flexure point away from the break off point (see figure 4), and an additional stiffness by virtue of the longitudinal loading, both of which tend to prevent the mass tipping.

3. The blade springs lie such that their long axis is close to being perpendicular to the longitudinal (x) direction. (see figure 1). They are narrow compared to their length to give a more compliant blade in the vertical direction, and this means that their lateral compliance, i.e. their compliance in the horizontal plane at right angles to their long axis, has a significant effect. Any lateral deflection of the wire caused for example by motion of the suspension in the longitudinal direction will lead to a lateral load on the blade tip, which will cause the blade tip to move laterally. That means in turn that the wire moves further laterally than would be the case with a laterally stiff blade. This is illustrated in figure 5, which shows the effect of a wire tension T acting at an angle. In the figure it can also be seen that the effective pivot point after a lateral translation is a smaller distance from the blade tip than the original flexure point. This in turn leads to a suspension that has less margin for stability in pitch than would be the case in a suspension with stubbier and hence laterally stiffer blades.

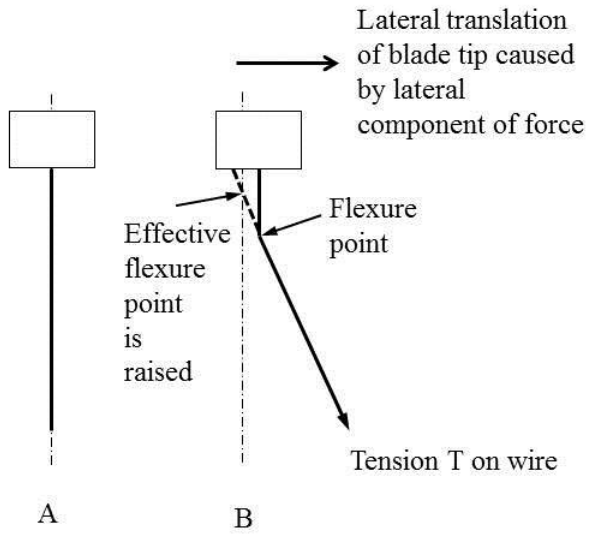

Figure 5. The oblong represents a blade tip seen end on, i.e. looking horizontally along the long axis of the blade from its tip. Diagram A shows a wire attached vertically to the blade tip. Diagram B shows the effect of lateral translation of the blade tip caused by a horizontal component of the tension T applied by the wire. The dotted line represents the original position of the wire attached to the blade. The effective flexure or pivot point of the translated blade/wire system is not the same as the flexure point of the wire. It has now been raised, reducing the margin for stability.

The first two of these effects were familiar from the GEO suspension design. However the LIGO blades are much narrower compared to their length than the GEO blades, and the lateral compliance effect was newly recognized.

2.6 Auxiliary components

The suspensions featured a number of auxiliary components, including earthquake stops to limit motions in case of earthquake, and fibre guards to protect the fibres from accidental damage during assembly. The earthquake stops for metal masses are made of stainless steel. For the silica masses they are made of fluoroelastomer with inserts of silica in order to avoid generation of static electric charges.

2.7 Prototyping

We took the design through four iterations of prototyping. Early prototypes demonstrated the feasibility of a four-stage suspension with three stages of blade springs for vertical isolation. The third round of prototyping, the so-called "noise prototype", included a monolithic final stage (i.e. silica test mass suspended on silica fibres) and allowed us to form a resonant cavity in our test interferometer at LASTI (LIGO Advanced Systems Test Interferometer at MIT). The final stage of prototyping used a spare noise prototype suspension and a modest number of individually made new parts, to check on final design changes.

2.7.1 Tilts and hysteresis in the wires

A feature arose during alignment of the masses in the noise prototype which became known as the "anomalous tilt" issue. We discovered that if a mass in the chain is tilted and then allowed to slowly recover, it does not always return to its starting position. Only if it was released some distance from the starting position and allowed to overshoot and settle, would the position be repeatable. As an example, a tilt of 25 mrad at the upper intermediate mass, gently released, would result in a static offset of ~1.3 to 1.5 mrad in the suspension. The effect was explored in some depth and was considered likely to be caused by hysteresis in the wires. The effect was only evident with large displacements: it did not prevent our control systems from working, although it could prove troublesome during alignment of the suspensions. In the final design we increased the stability of the suspension by modifying the distance between the breakoff points of the suspension wires and centre of mass, increasing the gravitational restoring torque and minimizing these effects.

2.8 Assembly process

The assembly process, in outline, is as follows. First the masses are assembled with their auxiliary parts. Metal substitute masses are used in place of the silica masses (test mass, compensator plate or end reaction mass, penultimate mass). They are adjusted to have the same mass as the silica masses that will eventually replace them, so that the deflections of the blade springs that support them will be consistent between metal and silica

assemblies. Wires are assembled under tension between clamps to give the correct lengths. The lower suspension (test mass, penultimate mass, upper intermediate mass) is made in separate chains and the two chains, with their lower structures less the sleeve, are mated together. The lower part of the suspension is assembled into the lower structure, and adjusted and balanced so that the two chains hang vertically, and the masses in the main chain are at the same height as those in the reaction chain. The top masses are assembled into the upper structure – because of the absence of the lower masses their blade springs must be held flat with special clamps. The two parts of the structure are mated together, and the chains are connected. Final adjustments are carried out to restore the chains to an aligned and balanced state. All of the OSEM flags are adjusted to align with the OSEMs, and the earthquake stops and other auxiliary parts are aligned. The cabling is put in place. At this stage the control system can be tested. The suspension may now be fitted to the seismic platform for further testing. The next stage is to break the upper and lower suspensions, break the lower suspension back into two chains, and substitute the monolithic final stage and the silica reaction mass for their metal counterparts. On reassembly, there is minimal readjustment to do because of the work already done with the metal substitute masses. The upper and lower suspensions are reunited and reassembled onto the upper stage and the sleeve is added to complete the suspension.

The suspension system and the internal seismic isolation system are normally fitted into the vacuum tanks as a single assembly. However, should any repair work be required, it is possible to split the suspension into upper and lower parts and remove just the lower part from the vacuum system.

3. Monolithic design for test mass suspensions

To achieve a thermal noise contribution of 10^{-19} m/√ Hz at 10 Hz, the suspension incorporates an ultra low mechanical dissipation lower stage between the penultimate mass and test mass. As previously mentioned, the use of monolithic suspensions was pioneered in GEO600 and, up to January 2012, a total of 160 years of fibre lifetime (10 years times 16 fibres) has been accumulated. This indicates the robustness of this technological approach. The 40 kg test mass in aLIGO is suspended using four fused silica fibres which are welded to small fused silica attachment standoff plates (“ears”). The ears are attached to the sides of the test mass by hydroxide-catalysis bonding. A detailed description of the monolithic reference design is given in Cumming et al. (2011a) and the following sections briefly describe the main techniques necessary to develop the aLIGO suspension.

3.1 Thermal noise considerations

Above the pendulum resonance the displacement thermal noise is given by (Callen and Welton 1951, Callen and Greene 1952)

$$x^2(f) = \frac{k_B T}{2\pi^3 m f}\left(\frac{f_o{}^2 \phi(f)}{f_o{}^4 \phi^2(f) + \left(f_o{}^2 - f^2\right)^2}\right) \qquad (3.1)$$

where T is the temperature, m is the pendulum mass, $\phi(f)$ is the mechanical loss angle of the pendulum, f_o is the resonant frequency, k_B is Boltzmann's constant and f is the frequency. To minimize the displacement thermal noise in room temperature instruments requires the use of ultra-low dissipation materials with low loss angle ($<10^{-8}$). In the aLIGO monolithic suspension the contributions to the loss angle, in order of importance, are from the fused silica fibre (Penn et al. 2006, Gretarsson et al. 1999, Cagnoli and Willems 2002), weld loss (Heptonstall et al. 2010) at the fibre/ear attachment point and mechanical loss associated with the ear-mass silicate bond (Cumming et al. 2011a). The fibre design is carefully chosen such that the thermoelastic loss is nulled at the bending point of the fibre. This requires a diameter of approximately 800 μm for a load of 10 kg per fibre, and results in the surface loss and weld loss contributing roughly equal amounts to the loss angle (Cumming et al. 2011a). Techniques to fully characterize the thermal noise of the full suspension have been developed by determining the bending energy stored in each portion of the suspension with ANSYS finite element software (Cumming et al. 2009). The loss terms at each point of the fibre are evaluated and scaled with the appropriate bending energy stored at that point in the suspension. In previous work good agreement (typically to within 15%) has been found between the measured loss for violin modes of fused silica suspensions and the predicted values from the finite element analysis (Cumming et al. 2011a).

The suspension fibre stores energy both in the elasticity of the material and the gravitational field. The gravity term is lossless and dominates in heavily loaded suspension fibres. Thus the pendulum loss is lower than that of the material used for the suspension fibre. This effect (Saulson 1990), which is termed dilution, is conveniently calculated in finite element software and is 90 for the pendulum mode of the aLIGO suspension (Cumming et al 2009). The resulting loss angle, corrected for dilution, is used to calculate the thermal displacement noise in equation (3.1).

3.2 Ear Design and Silicate bonding

Fused silica ears facilitate the attachment of the fused silica fibres to the sides of the penultimate and test mass, which are made with flat sections on the sides for this purpose. Figure 6 shows a schematic of the lower monolithic stage. The ears, made from Heraeus Suprasil 312, are bonded onto the side of the mass with hydroxide-catalysis bonding (Rowan et al. 1998, Elliffe et al. 2005). The technique requires that the initial bonding surfaces are flat to within 60 nm and this is achieved through a combination of mechanical and magnetorheological polishing (detailed in van Veggel et al., 2009). After the mass and ear are thoroughly cleaned, as detailed in van Veggel et al. 2012, a sodium silicate solution is applied to the interface between the ear and test mass which locally starts to etch the glass surfaces.. During the etching process the pH of the solution begins to drop until at pH <11 the bond solution begins to polymerise and produce a strongly cross-linked structure. The final stage of the bond process is the dissipation of water

which occurs at the surface of the bond over a period of 1 month. Previous studies (Cunningham et al. 2010) have shown that the thermal noise associated with the bonded ears is consistent with the noise budget for technical noise sources (Fritschel et al. 2009).

Each ear has a pair of horns which are the locations where the fibres are welded. The pyramidal shape of the horn (see figure 6) ensures that sufficient heat can be applied to the weld region. Finite element analysis was performed to ensure that both the shear stress and peeling stress were sufficiently low (van Veggel et al. 2009). The shear stress of 0.16 MPa is determined by the bond area (60 mm x 20 mm) and is well below the ultimate strength measured in experimental studies which is typically >2 MPa (Elliffe et al. 2005). The symmetric design of the horn ensures that the peeling stresses are <1 MPa and that bending of the horn under the applied load is insignificant.

3.3 Fibres and Thermal Noise Performance

The aLIGO reference design requires that the fused silica fibres are dumbbell shaped in order to maintain the requisite thermal noise performance whilst ensuring that the suspension bounce mode is <10 Hz and the first violin mode is above 400 Hz (Barton et al. 2008). As mentioned previously, a fibre diameter of 800 μm ensures that the static stress at the bending point nulls the thermoelastic contribution. The remainder of the 600 mm long fibre is reduced to 400 μm in diameter in order to increase the violin mode frequency to approximately 500 Hz and reduce the highest vertical mode frequency to ~ 9 Hz. The stress in this section of the fibre is approximately 800 MPa which is a factor of 6 below the typical breaking stress of the fibre (≈5 GPa) (Tokmakov et al. 2012). The fibres are produced with a CO_2 laser pulling method (Heptonstall et al. 2011) which ensures a good dimensional tolerance of the suspension fibres and the ability to accurately control the fibre geometry. The fibres are pulled from 3 mm diameter precision Heraeus Suprasil 2 stock (see figure 7) which has a low number of surface voids and a dimensional tolerance of 3 mm +0.06/-0.01 mm. An initial laser polishing step is used in order to heal surface cracks. This increases the breaking strength of both the residual stock, used to weld the fibre to the ear, and the fibre itself. The fibres are produced using the feed-pull method (Heptonstall A, et al. 2011) where the fibre geometry can be adjusted by varying the speed of the feed and pull motors.

After pulling, each fibre is measured with a non-contact optical profiler (Cumming et al. 2011b) in order to allow the fibre geometry to be imported into ANSYS for the thermal noise prediction. This important step allows an accurate prediction of the thermal noise and bending points of a realistic suspension. Each fibre is then stored in an evacuated enclosure.

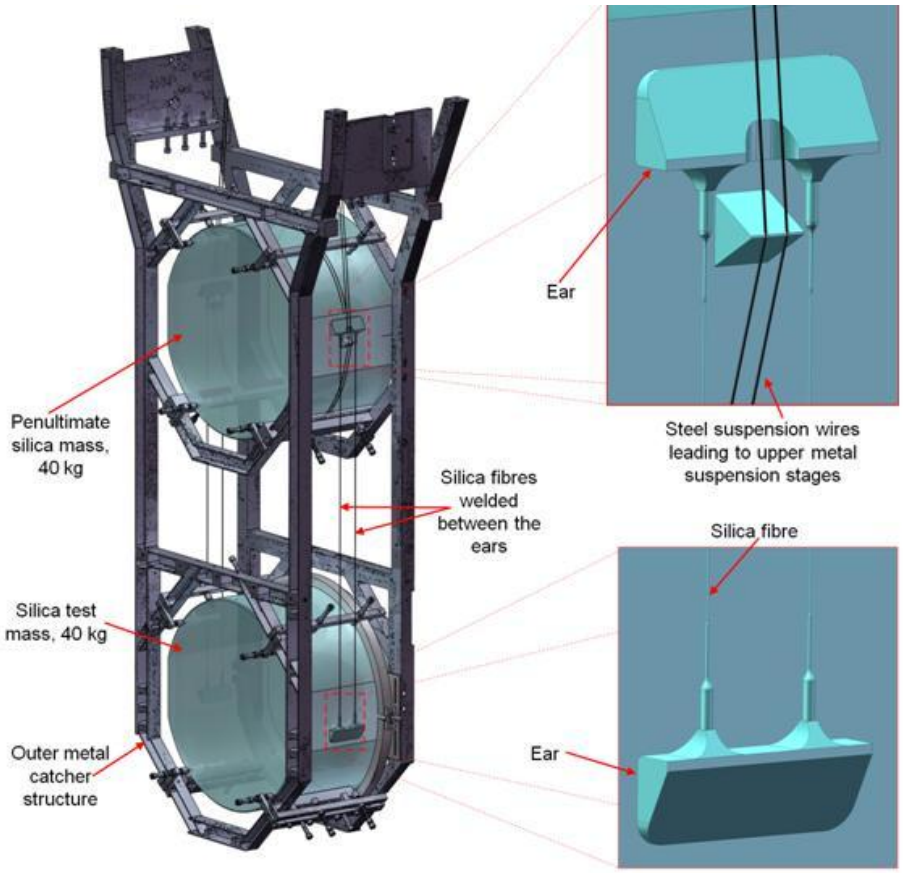

Figure 6 Monolithic stage of the quadruple suspension showing the location of the ears and fused silica fibres (adapted from Cumming A V et al. 2011a).

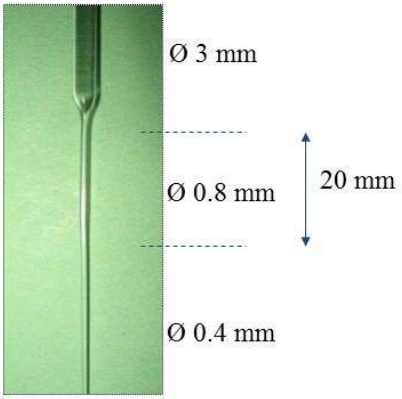

Figure 7. Photograph of the end of a fibre showing the diameters of the various stages.

The predicted thermal noise of the fused silica lower stage as a function of frequency is shown in figure 8. Above the pendulum modes of the quadruple suspension (> 4 Hz) this

noise is dominated by the silica stage alone and thus the finite element model gives an accurate thermal noise prediction. At 10 Hz the total displacement noise meets the requirement of 10^{-19} m/√ Hz at 10 Hz, for each test mass.

3.4 Welding

Four fused silica fibres (8 welds) are required for each suspension. Prior to welding, each fibre is proof tested by supporting 15 kg for 15 minutes. This is sufficient to cause any fibres which may have been accidentally touched to fail at this point. The fibre is then placed into a cutting jig which is used to adjust the length of the fibre by scribing off excess 3 mm stock at either end. This allows the bending point of the suspension (described in section 2) to be positioned to an accuracy of approximately 1.5 mm, which results from the variation between fibre geometries and the accumulated tolerance in measurement. For the aLIGO suspensions a total fibre length of 610.6 mm is required between the ends of the weld horns. An allowance of an extra 1 mm of material is made at each end in the cutting, and this is consumed in the weld. The 3 mm fibre stock is held at each end with zirconia tipped tweezers which are attached to a 3-axis translation stage. The stage allows accurate positioning of the fibre during welding. Welding is performed with a CO_2 laser which is directed to the weld region via an articulated arm and mirror galvanometers, allowing the beam to be aligned in any orientation. During welding the silica stock/horn are heated close to their boiling point (2250 ^{o}C) and extraction is used to remove any silica vapour from the weld region. Once the fused silica stock softens, it is fed in towards the horn to form a butt weld. The translation stages which hold the fibre allow the fibre to be translated and/or rotated to remove any misalignment which may occur during the feeding of the fibre into the weld. Heating is applied until the weld region forms a clear meniscus and no sharp edges are visible. Each weld typically takes 10 minutes and this procedure is repeated for the remaining 7 welds.

An annealing procedure is applied to the 4 welds at the penultimate mass and the 4 welds at the test mass before hanging the test mass. This ensures that all fibres carry an identical load and that the welds are aligned vertically. The test mass is lowered (on a jack) by 0.35 mm which introduces a tension of ~6 N into each fibre. An autocollimator is also used to measure and adjust the test mass pitch to be equal to the penultimate mass pitch. Each of the 4 welds at the penultimate mass are then heated, in turn, to their softening point in order to relieve the tension. This is followed by laser polishing of the 3 mm stock in the region where the tweezer tips have made contact with the stock, to remove any surface cracks. The procedure is then repeated for the 4 test mass welds. The test mass is then lowered and the fibres stretch an additional 6 mm under the 40 kg load. After hanging, the pitch of the test mass relative to the penultimate mass is monitored. Due to the accuracy of aligning the fibres onto the horns (<0.2 mm) and the accuracy of bonding the ear onto the masses (<0.1 mm) the pitch is typically within the range ±2 mrad.

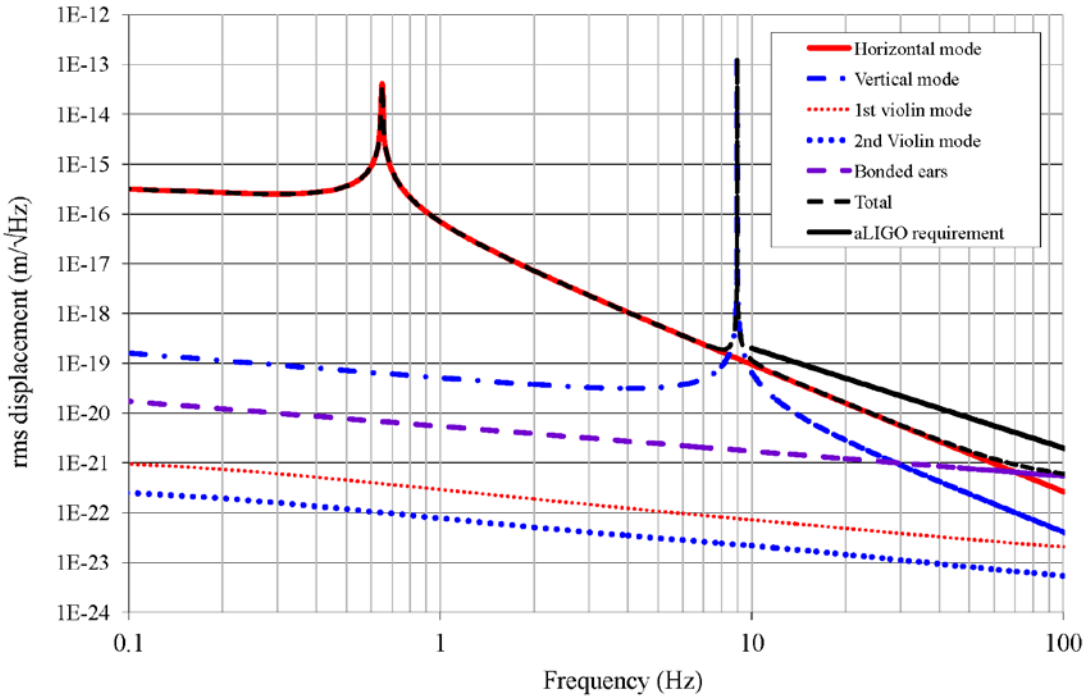

Figure 8. Displacement thermal noise spectra for the monolithic stage of a single aLIGO monolithic suspension (adapted from Cumming et al. 2011a). The total noise is made up from the quadrature sum of contributions from the horizontal pendulum mode, the vertical mode with a vertical-horizontal cross coupling of 0.1%, the first two violin modes and silicate bonding of the attachment ears (see section 5 for comment on the cross-coupling value). The thermal noise requirement curve, which is defined from 10 Hz and above, is also shown. The requirements curve is for the quadrature sum of longitudinal and coupled vertical thermal noise, each of which is 10^{-19} m/√Hz at 10 Hz. Not shown is the thermal noise contribution from upper stages of the quadruple suspension, which falls below the noise from the monolithic stage by 10 Hz.

4. Damping and control

4.1 Advanced LIGO sensors and actuators

Relative displacement sensors provide a simple and convenient method of measuring the position of an object, or "flag", which can be attached to a test mass. They usually are comprised of an LED emitter, photodiode detector, and either a focusing optic in the case of an imaging sensor, or an opaque flag in the case of a shadow sensor. The flag is used to obscure a proportion of the emitted beam from becoming incident upon the detector, and is the scheme previously employed in the initial LIGO sensor. However, this scheme has now been refined for aLIGO to enable large scale production of ultra high vacuum compatible units, which offer improved assembly reliability, and ease of alignment.The significantly heavier test masses used in the aLIGO suspensions have given rise to two variants of the sensor and actuator units: the "Birmingham Optical Sensor and Electro-Magnetic actuator", or BOSEM (Carbone et al 2012), that accommodates a larger magnet and provides larger actuation force than the smaller "Advanced LIGO OSEM", or AOSEM, which is closer to the initial LIGO sensor design. The BOSEM actuator coil is comprised of 800 turns of polyimide coated 32-AWG wire, wound around a coil-former, and is capable of generating peak actuation forces of up to 125 mN. The corresponding magnet, of either Nd:Fe:B or Sm:Co material [1], is cylindrical of 10 mm diameter and 10 mm long.

The BOSEM sensor incorporates an infrared LED with peak emission at 950 nm (clear of the main interferometer wavelength of 1064 nm) and a single element photodiode, both mounted in conventional hermetically sealed, stainless steel packages. To reduce magnetic coupling between these sensor packages and the actuator, it is necessary to separate the sensing location and the sweet spot of the actuation coil where the force is at a maximum. A rectangular flag, approximately 24 mm long, extends between the sensor and the magnet which is placed at the actuator sweet spot. The infrared LED package contains an integral lens, however, an additional external lens is used to improve the collimation of the beam, whilst a slotted mask measuring 1.4 x 4.5 mm intercepts the beam, ensuring only paraxial rays contribute to the noise floor. Misalignment of the suspended components could lead to light passing the sides, rather than the end of the flag. This is eliminated by widening the flag to ensure it is wider than the mask described above (the rectangular flag has a width of 5 mm, and is 2.5 mm thick [2]). The linear peak-to-peak operating range is 0.7 mm. Performance is limited at low frequencies by 1/f noise inherent to the infrared LED, and at frequencies above a few Hertz by shot-noise in the resulting photocurrent. Key assemblies, mounting and adjustment fixing, as well as the overall dimensions of the BOSEM are highlighted in Figure 9.

Following a period of development and refinement of the quadruple suspension design and the associated active damping scheme (see below), the sensitivity required for the Advanced LIGO sensor was determined to be 3×10^{-10} m $Hz^{-1/2}$ at 1 Hz, falling to 10^{-10} m $Hz^{-1/2}$ at frequencies of 10 Hz and higher. The design met the low frequency goal and yielded a shot noise limit of typically 7×10^{-11} m $Hz^{-1/2}$ by 10 Hz.

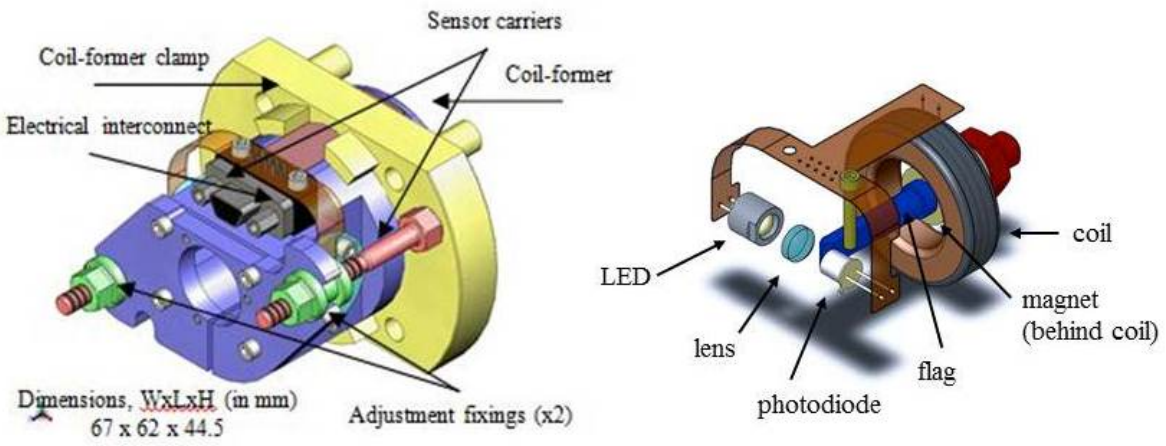

Figure 9. CAD renderings of the BOSEM assembly. The right hand drawing shows the inner assembly. The infrared LED projects a beam of light across the central aperture where it may be interrupted by a flag attached to the mass before reaching a photodiode on the opposite side.

[1] Samarium cobalt is used in the most noise-critical locations as it has lower Barkhausen noise. (Weiss 2009)

[2] This design replaces a narrower profile cylindrical flag, which was observed to couple lateral motion in the presence of sufficient misalignment of the suspended components.

All production BOSEMs were characterized, by operating them with a fixed flag, to check that sensor performance met the requirement. Although the shot noise limited performance was achieved consistently, obtaining the required performance at 1 Hz necessitated screening every infrared LED. A large variation in the 1/f photo-current noise was observed from batch-to-batch, resulting in a screening rejection rate of approximately 75%. The best devices were incorporated into BOSEMs, which then all met the required standard.

As noted below, an actuator with lower force and hence lower noise coupling is required for the penultimate stage. This was accomplished by modifying the initial LIGO OSEM, producing the so-called AOSEM. The sensing capabilities of this device have no role in the quadruple suspension and so are not described here. By reducing the number of turns to 400 on a coil of 25 mm O.D. and 4 mm long with a smaller magnet (2 mm dia. by 6 mm long), the peak force is reduced to 0.7 mN.

4.2 Local control

Control of the interferometer is traditionally divided into a *global* system plus one *local* subsystem per suspension. The global control acts to adjust relative positions and alignments of suspended components, taking as inputs information extracted from interferometric measurements. In contrast the local control systems damp or cool the rigid-body modes of the suspensions, using signals obtained from displacement sensors (BOSEM sensors) arrayed around the top mass suspension. A schematic diagram showing the basic layout of local and global control actuation is shown in figure 10.
The use of low-dissipation materials leads to high quality-factors, Q, for the rigid-body modes. These modes are excited to varying degrees by residual motion of the suspension point from which the whole suspension is hung and possibly by the action of the global control system. If left un-damped the residual *rms* motion would be enhanced by $\sqrt{Q}$ for each mode, leading to amplitudes beyond the limit for operation of the global interferometer control. Therefore these modes require to be damped.
The use of passive damping was investigated in the form of eddy current dampers (Plissi et al. 2004) consisting of magnets attached to the top stage of the suspension moving within cylindrical recesses in copper blocks fixed to the support structure. This method suffers from slightly too high (thermal) noise for the desired amount of damping. In prototype testing it became apparent that the 1 mm clearance between the copper and magnets produced a substantial risk of mechanical interference and considerably slowed construction of the suspension assemblies. Active damping, based on the low-noise BOSEM sensors described in section 4.1, can meet damping and noise requirements, and has been selected as the damping technique for aLIGO.

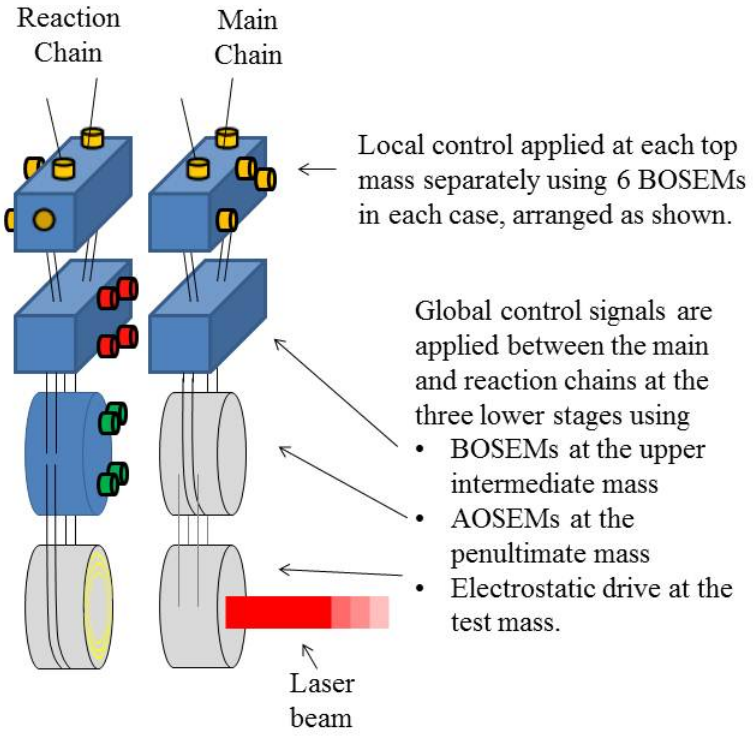

Figure 10. Diagram illustrating how local and global control signals are applied. Electrical wiring is not shown. The wiring is routed up the reaction chain in a manner that minimizes additional stiffening.

The idea is to sense the motion of the top mass of each suspension with respect to the support structure using 6 sensors to cover the 6 degrees of freedom, to digitise and filter the signal, and to apply the resulting correction force *via* the coil-magnet actuators again at the top mass. Sensing and actuation at the top mass carries the benefit that the lower 3 stages help to filter any residual noise at frequencies above the eigenmodes of the suspension. Even so, a simple differentiator-law filter would allow far too much sensor noise to be fed back at the lower end of the sensitive band of the interferometer (near 10 Hz), so more sophisticated techniques that include low-pass filtering are needed.

The method developed for aLIGO combines a refinement of the technique previously employed in GEO600 with a new idea – modal damping – derived from modern control theory. These techniques are explained in Strain and Shapiro (2012). Modal damping is an optimal approach offering the best balance between strength of damping and residual noise at the test mass. However the older approach, which is not so finely-tuned to each individual suspension is more robust against minor fabrication and construction tolerances. For this reason we have selected modal damping for use in the critical *x*-axis (along the interferometer arm), for which the noise requirements are most stringent, while the other technique is applied for the remaining coordinates; its robustness allowing more rapid deployment across the many quadruple suspensions. Fortunately the *x*-direction

dynamics show relatively low sensitivity to parameter variation, so setting up modal damping in *x* should not be burdensome.

As noted above, much of the required filtering of noise from the local controls is provided by the lower 3 stages of the suspension (i.e. about 6 orders of magnitude filtering from longitudinal displacement of the top mass to longitudinal displacement of the test mass at 10 Hz). The remaining filtering necessary to bridge the gap from the sensor noise, typically 7×10^{-11} m $Hz^{-1/2}$, to the technical noise budget for longitudinal motion of one suspension of 10^{-20} m $Hz^{-1/2}$ is provided by the controller.
The resulting design provides a damping time (i.e. the time for the amplitude to decay by a factor *e*) of around 10 s for all the rigid-body modes (except the two involving extension of the silica fibres – these modes are barely excited by external forces and are un-damped). This allows the suspension to recover from even large disturbances in a matter of minutes.

4.3 Global control

The interferometer must be held quite precisely to the correct operating point, within a small fraction of a picometre. This involves controlling the lengths of the arm cavities by actuating on the suspended end and input test mass optics which are supported by the quadruple suspensions. The signals required for this control are obtained by interferometric means and processed by the Control and Data System (CDS), the details of which are beyond the scope of this paper (see Bork et al. 2011). The actuation systems required to apply the control forces to the suspended masses are considered part of the suspension and so are described here along with their basic principles of operation. See figure 10.

The interferometric sensing provides information that allows for longitudinal, yaw and pitch control of each optic (test mass). The other 3 degrees of freedom do not couple as strongly to the interferometer and are dealt with by a combination of passive filtering (i.e. isolation from the ground) and local damping.

Long-term operation in the presence of Earth-tides requires long-range actuation (see for example Raab and Fine 1997). On the other hand the control system is required to operate within the technical noise limit (i.e. 10^{-20} m/√Hz at 10 Hz, even less at higher frequencies) for the longitudinal direction, so *hierarchical* control, by which small range high frequency and long range low frequency signals are applied separately, is required to accomplish this with electronic systems of finite dynamic range. The quadruple suspension, along with its suspended reaction chain which acts as a quiet platform for actuation, provides a convenient basis for the application of hierarchical control.

At the lowest stage the smallest-amplitude and highest-frequency corrections are directly applied to the test mass. This is achieved using an electrostatic actuator (also termed an electrostatic drive – ESD) consisting of a segmented pattern of strip-electrodes which form 4 interleaving sets (see figure 11). These patterns, coated in gold over chromium on the face of the fused silica end reaction mass and compensator plate, the lowest masses in

the two types of reaction chains, produce a fringing field which penetrates the dielectric bulk of the test mass. The capacitance of the electrode pattern then depends on the distance between the test mass and the reaction mass, so changing the voltage on the electrodes changes the attractive force between the masses. The force depends on the energy stored in the capacitor, and hence on the square of the applied voltage. Linearization is achieved by adding control signals on to a suitable bias voltage. Further correction of the large signal response is possible by appropriate programming of the CDS to compensate for residual nonlinearity. Segmentation of the electrodes into 4 patches allows pitch and yaw control as well as longitudinal actuation. Most of the ESD actuation will be done at the end test masses where the gap is 5 mm, a size comparable to the spacing of the electrodes. The ESD, developed from a design which has operated in GEO600 for many years, is described further in Strain 2006.

Due to the transmissibility of the suspension dropping rapidly towards higher frequencies, the burden for control falls mainly in and below the frequency band occupied by the rigid body suspension modes. The electrostatic drive can be adjusted in strength such that the electronic noise (largely from the digital to analogue converters – DACs – of the CDS) falls below the noise limits for the suspension. The dynamic range in a 1 Hz bandwidth is as much as 160 dB, but even so the range of the ESD is limited to of order picometres (essentially the 10^{-20} m/√Hz of the requirement times 10^{8} voltage ratio, or 160 dB). This leads to a requirement for peak forces in the micronewton range. That suffices for the frequency range above about 5-10 Hz, but for lower frequencies a stronger actuator is required to provide larger corrections. The choice of electrostatic actuation at the test mass level was driven by the need to avoid extra attachments to the test masses which could increase mechanical dissipation and increase thermal noise. In addition there would be a risk of magnets interacting with stray fields potentially leading to unwanted forces.

The actuators fitted to the penultimate (PUM) stage benefit from additional noise filtering in the operating frequency band of the interferometer (by approximately a factor of 200 at 10 Hz, for example, and progressively more toward higher frequencies), but suffer from a bandwidth limit due to the same 2-pole low pass effect of the lowest stage of the suspension. Thus actuators at the PUM stage can complement but not replace the ESD. The AOSEM design (see above) employs magnets sized such that stray alternating magnetic fields are not expected to lead to excessive motion of the suspension. Again a set of 4 actuators allows for pitch and yaw as well as longitudinal actuation. These actuators cover the range from of order 1 Hz up to about 10 Hz, over which the spectral density of the force signals they must provide varies by many orders of magnitude. To extend the effective dynamic range far beyond that provided by the driving DACs, suitable shaped filtering is provided between the DAC output and the circuit which generates the current needed for the actuator. By this means the PUM AOSEMs can provide forces large enough to operate down to around 1 Hz in normal operation, where the amplitudes are in the nm range.

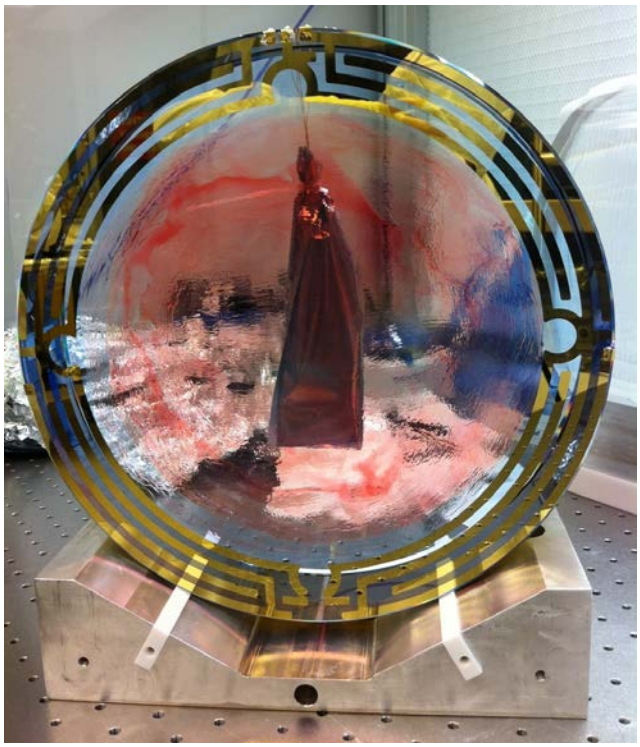

Figure 11: Photograph of the compensator plate showing the pattern of the ESD electrodes. The inner diameter is left free to transmit light. The electrodes are formed by evaporation of gold over chromium on to a fused silica substrate. Connections are made by soldering fine wires. One set of electrodes are electrically commoned, the other set is separated into quadrants to allow longitudinal, pitch and yaw actuation. The actuator is driven from a low-noise high-voltage (800V) source to provide up to micronewton forces. The pink colour in the picture is due to a protective coating of First Contact™ (Photonic Cleaning Technologies) which will be removed before operation. The central bag temporarily holds the connector attached to the wires. When the mass is hung in its suspension the connector gets attached to five-way cable at the mass above.

Still-lower frequencies are dealt with by additional hierarchical stages further up the suspensions. A set of 4 BOSEMs is provided at the upper intermediate or UIM stage, with up to of order micron range, and finally the very slowest signals are fed to the two-stage internal isolation system (ISI) and the hydraulic external pre-isolator (HEPI) system (Abbott et al. 2004) which provides up to 2 mm peak-to-peak adjustment range on longer timescales, providing for indefinite operation.

5. Expected performance

The expected thermal noise performance was shown in figure 8 in section 3. As noted in section 3.1, we have seen good agreement between measured and modeled losses for violin modes in prototype monolithic suspensions, which gives us confidence in the thermal noise modeling. A direct measurement of thermal noise performance will require a full interferometer with good sensitivity.

As there are no local sensors at the test mass stage, we must rely on a dynamical model of the suspension in order to predict the residual motion until global sensing becomes available. We are able to excite and measure 22 of the 24 rigid-body, resonant modes from the top stage of the suspension. Thus measuring the response of the top stage sensors to excitation in all six degrees of freedom at the top mass and comparing against the predicted response from our model is sufficient to confirm the model's accuracy in predicting the response at all stages to drive at all stages (Shapiro 2011). Figure 12 shows the measured response of the top mass chain to actuation at the top mass in the longitudinal direction for two first article suspensions, compared against our model. We see that the agreement is very good. We have repeated such measurements in all degrees of freedom and have confirmed agreement with our model for all 22 low frequency modes of the quadruple suspension. In addition we have confirmed that we can lower the quality factor of all these modes to a suitably low value (Q ~ 10) for global feedback to operate.

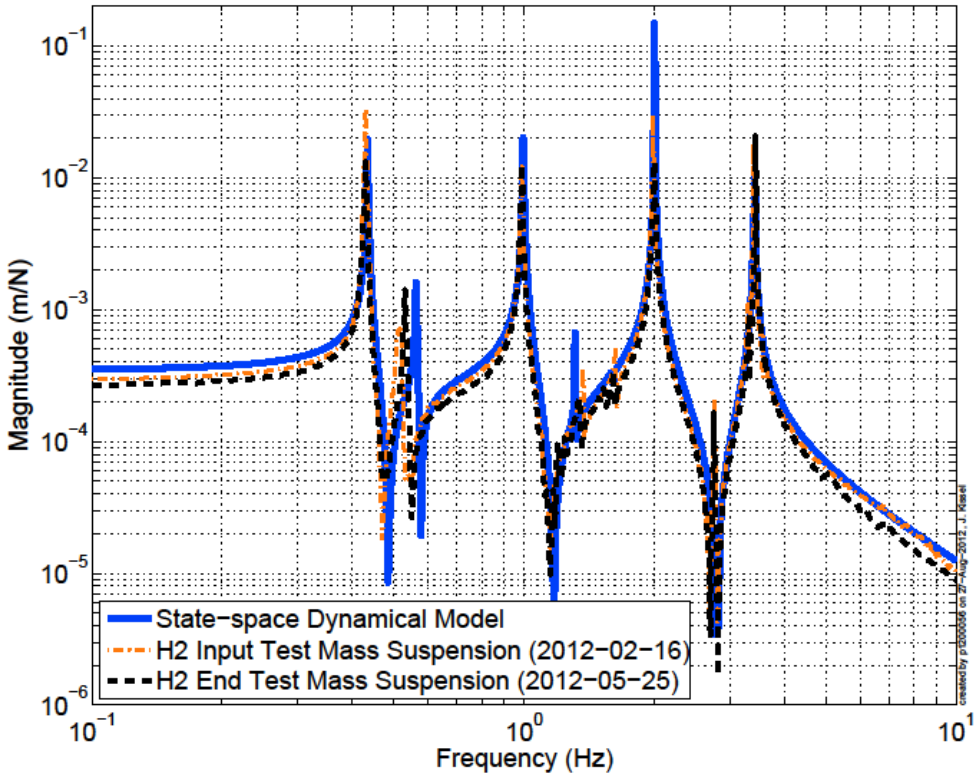

Figure 12: Modeled and Measured, top mass displacement response to longitudinal top mass excitation. For the two measurements, the modes at 0.43, 1.00, 2.01, 3.42 Hz whose mode shapes are primarily in the longitudinal direction, agree with the model to within 1%. All other modes seen in response, at 0.56, 1.31, and 2.81 Hz are modes primarily in the pitch direction, which can vary greatly in frequency with small changes to the mechanical construction. These modes agree with the model to within 10%, but their measured mode frequencies are consistent to within 2%. The accuracy of the resonant magnitude is limited by the resolution of both the model and measurement resolution; the overall magnitude agrees to within 25% with the model, and 10% between measurements. The measured response in the five other degrees of freedom agree with the model to within similar, if not better, accuracy.

With this affirmed dynamical model, we can then predict the response of the test mass to residual seismic motion at the suspension point, with active damping loops engaged. Using this response, we predict the displacement of the test mass by taking as the input to the suspension point the current expected noise performance on the final stage of the internal two-stage isolation system, the BSC-ISI (Matichard et al. 2010) from which the suspension is hung. Figure 13 shows this expected performance in the X (longitudinal, parallel to the cavity axis) and 10^{-3} x Z (vertical, parallel to local gravity) directions, where 10^{-3} is the assumed cross-coupling factor betweeen the vertical and longitudinal directions. We also show the quadrature sum of X and 10^{-3} Z. We take 10^{-3} as a conservative estimate of the cross-coupling factor. There is a small inherent cross-coupling of vertical to longitudinal due to the curvature of the Earth over the 4 km arm lengths of LIGO, since verticals defined by local gravity at each end of an arm are not parallel at a level of 6 x10^{-4} radians. Further cross-coupling will be introduced via mechanical imperfections in the suspension. However from analysis, these effects have been shown to be small (Husman et al 2000). Motions in the other degrees of freedom are estimated from modeling to give less longitudinal motion than the X and Z contributions. Also shown in figure 13 is the seismic noise requirement for the quadruple suspension in conjunction with the BSC-ISI.

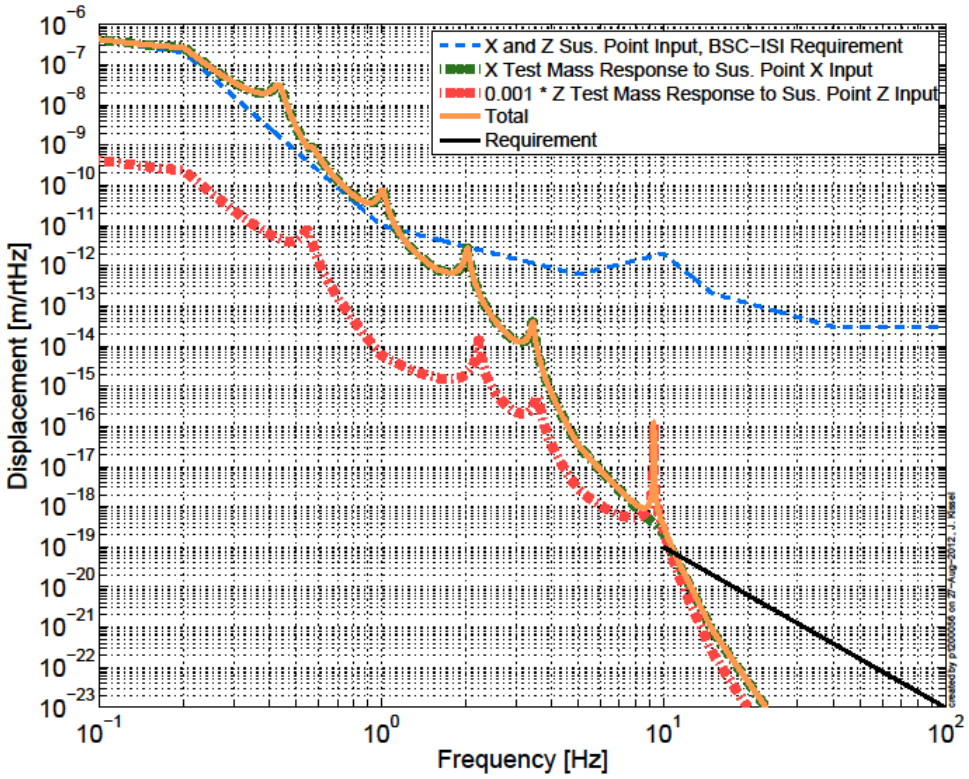

Figure 13. Expected residual seismic motion at the test mass of the quadruple suspension, derived as explained in the text. The blue (dash) line shows the expected input from the BSC-ISI at the suspension point to the quadruple suspension. The green(solid) line, mostly hidden under the gold line, shows the longitudinal (X) motion. The red (dot-dash) line shows the vertical (Z) motion multiplied by a factor of 0.001.The gold (solid) line shows the quadrature sum of X and 0.001 Z. The black (solid) line shows the seismic noise requirement which is defined from 10 Hz and above.

The high-Q, resonance seen at 9 Hz is one of the 2 undamped modes of the suspension. (The other is a roll mode at ~13 Hz.) The noise at 10 Hz is just above our requirement of 10-19 m/rtHz, due to a combination of the shoulders of the 9 Hz resonance and an enhancement of residual noise on the internal isolation system around 10 Hz caused by bending modes of the vacuum chamber support structure upon which the BSC-ISI is mounted. As these two features are limiting the performance, several options are being explored to reduce their contribution including local feedback at lower stages of the suspension (for the 9 Hz mode), feed-forward control on the BSC-ISI, and external mechanical stiffening / damping (for the support structure resonances). Contributions to the above displacement prediction notably do not include higher-order, non-rigid body, high-Q modes of the suspension (specifically the first fundamental or "violin" modes of the suspension fibers, at ~500 Hz) as well as technical noise contributions such as actuator and sensor noise. We require displacement due to technical noise to be a factor 10 below the expected residual seismic motion at 10 Hz and modeling of those noise sources using the most up-to-date configuration of their design is ongoing.

6. Other Suspensions

We have discussed in detail the design features of the test mass suspensions, which are the most stringent in terms of performance. Suspensions for the beamsplitter, the input modecleaner, the power and signal recycling cavity mirrors and the output modecleaner are similar in design but incorporate fewer stages (triple or double) depending on the required isolation. The thermal noise requirements are such that steel music wire can be used in the final stage of each suspension rather than fused silica, though care must be taken to achieve a clean breakoff at the top and bottom of the final wire suspension to minimise rubbing friction. Finally there is no need for a quiet reaction chain from which to apply actuation forces for these suspensions due to the more relaxed noise requirements.

7. Current Status

At the time of writing, suspensions are being assembled at both observatories. Installation has started at the LIGO Hanford Observatory (LHO) and is expected to start at LIGO Livingston Observatory in autumn of 2012. Fig 14 shows the first two production quadruple suspensions with monolithic final stages at LHO. The gold barrel of the compensator plate in the reaction chain can clearly be seen on the left. The first experiments involving two quadruple suspensions forming the ends of a single 4 km arm at LHO were started in July 2012.

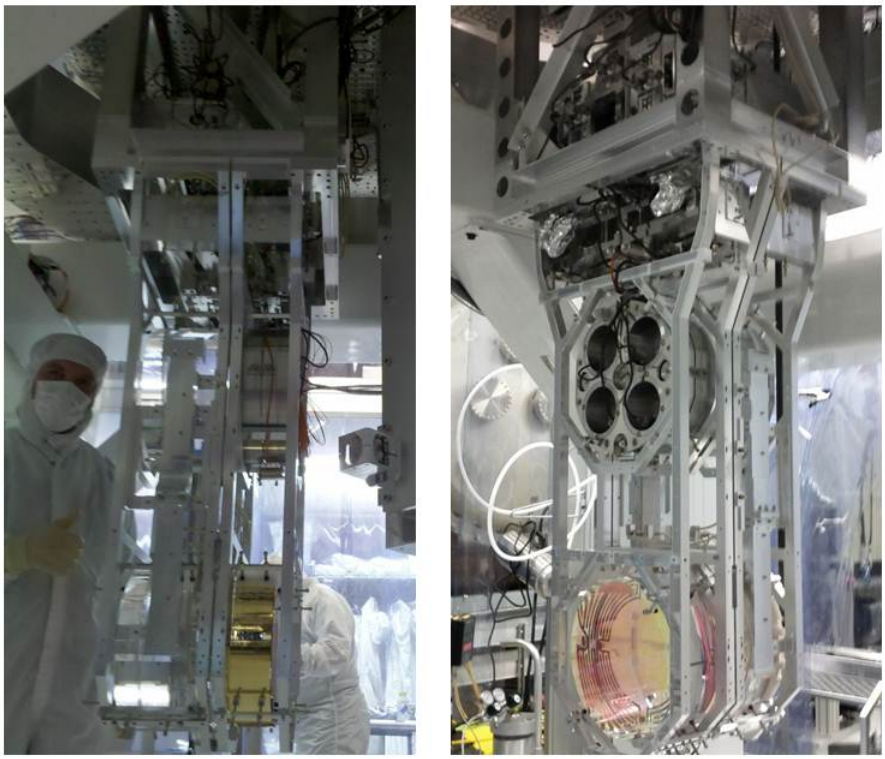

Figure 14 Photographs of the first two production quadruple suspension systems ready for installation in aLIGO. On the left is an input test mass suspension suspended from the isolation system. The gold-coated barrel of the compensator plate can be seen. On the right is the first of the end test mass suspensions.

Acknowledgments

The authors wish to acknowledge the many colleagues in LIGO and the LIGO Scientific Collaboration who have supported this work. In particular we acknowledge the outstanding work of the Suspensions mechanical and electronics assembly, installation and testing teams at the LIGO Hanford and LIGO Livingston observatories, Caltech and MIT, and also members of the LASTI staff at MIT who supported the prototype work there. In addition the work would not have been possible without the support of LIGO management, procurement and quality assurance teams, and colleagues in other subsystems of Advanced LIGO including Systems, Seismic, Core Optics, Facilities Management and Control and Data Systems. We also acknowledge the inputs from colleagues who have given feedback and made suggestions for improvements to the design, both formally at the various design reviews over the last few years and informally as issues arose. We would like to thank the National Science Foundation in the USA (award Nos. PHY-05 02641 and PHY-07 57896). LIGO was constructed by the California Institute of Technology and Massachusetts Institute of Technology with

funding from the National Science Foundation and operates under cooperative agreement PHY-0107417. In the UK, we are grateful for the financial support provided by Science and Technology Facilities Council (STFC), the University of Glasgow, the University of Birmingham, the University of Strathclyde and the Rutherford Appleton Laboratory. This paper has LIGO document number LIGO- P1200056-v3.

References

Abbott R et al. 2004 *Seismic isolation enhancements for initial and Advanced LIGO,* Class. Quantum Grav. **21** S915–S921

Ballmer S et al. 2007 *Advanced LIGO Interferometer Sensing and Control Conceptual Design*

Barton M 2006 *Models of the Advanced LIGO Suspensions in Mathematica*™, LIGO document T020205-02D
https://dcc.ligo.org/public/0010/T020205/001/T020205-02.pdf

Barton M et al. 2008 *Proposal for baseline change from ribbons to fibres in AdvLIGO test mass suspension monolithic stage.* LIGO Document T080091-00
https://dcc.ligo.org/public/0027/T080091/000/T080091-00.pdf

Beccaria M et al. 1998 *The creep problem in the VIRGO suspensions: a possible solution using Maraging steel,* Nuclear Instruments and Methods in Physics Research A **404** 455-469

Biscans S and Matichard F 2010 *Passive damping solutions for the BSC-ISI and Quadruple Pendulum structural modes* LIGO document G1000815-v1
https://dcc.ligo.org/public/0020/G1000815/001/Passive_Damping_LVC_Poster_Sept_2010.pdf

Bork R, Aronsson M, Barker D, Batch J, Heefner J, Ivanov A, McCarthy R, Sandberg V And Thorne K *New Control and Data Acquisition System in the Advanced LIGO Project* LIGO document P1100052
https://dcc.ligo.org/DocDB/0060/P1100052/003/LIGO-P1100052.v2.pdf

Braccini S et al. 2000 *The maraging-steel blades of the Virgo super attenuator* Meas. Sci. Technol. **11** 467–476.

Callen, H B and Welton T A 1951, *Irreversibility and Generalised Noise.* Physical Review **83** 34-40.

Callen, H B and Greene R F 1952, *On a Theorem of Irreversible Thermodynamics.* Physical Review **86** 702-710.

Cagnoli G and Willems P 2002, *Effects of nonlinear thermoelastic damping in highly stressed fibres,* Phys, Rev, B **65** 174111

Carbone L et al. 2012 *Sensors and Actuators for the Advanced LIGO Mirror Suspensions,* Class. Quantum Grav. **29** 115005

Cavalleri A et al. 2009 *Gas damping force noise on a macroscopic test body in an infinite gas reservoir,* Phys. Rev. Lett. 103, 140601

Cumming A, Heptonstall A, Kumar R, Cunningham W, Torrie C, Barton M, Strain K A Hough J and Rowan S 2009, *Finite element modelling of the mechanical loss of silica suspension fibres for advanced gravitational wave detectors,* Class. Quant. Grav, **26** 215012

Cumming A V et al. 2011a, *Design and development of the advanced LIGO monolithic fused silica suspension* Class. Quantum Grav. **29** 035003

Cumming A V et al. 2011b, *Apparatus for dimensional characterization of fused silica fibers for the suspensions of advanced gravitational wave detectors.* Rev. Sci. Instr., **82** 044502

Cunningham L et al. 2010 *Re-evaluation of the mechanical loss factor of hydroxide-catalysis bonds and its significance for the next generation of gravitational wave detectors.* Physics Letters A, **374** 3993-3998

Elliffe E J, Bogenstahl J, Deshpande A, Hough J, Killow C, Reid S, Robertson D, Rowan S, Ward H and Cagnoli G 2005 *Hydroxide-catalysis bonding for stable optical systems for space.* Class. Quant. Grav., **22** S257-S267

Fritschel P for the Advanced LIGO Systems Group 2009, *Advanced LIGO Systems Design* LIGO document T010075-v2
https://dcc.ligo.org/public/0005/T010075/002/SysDesign.pdf

Gossler S 2004 *The suspension systems of the interferometric gravitational wave detector GEO600,* PhD Thesis University of Hannover

Gretarsson A and Harry G M 1999, *Dissipation of mechanical energy in fused silica fibers.* Rev. of Sci. Instr., **70** 4081-4087

Gwo D-H 2001 *Ultra precision and reliable bonding method* United States Patent no US 6284085 B1

Harry G M and the LIGO Scientific Collaboration 2010, *Advanced LIGO: the next generation of gravitational wave detectors* Class. Quantum Grav. **27**, 084006

Heptonstall A et al. 2010 *Investigation of mechanical dissipation in CO2 laser-drawn fused silica fibres and welds.* Class. Quantum Grav., **27** 035013

Heptonstall A, et al. 2011 *CO2 laser production of fused silica fibers for use in interferometric gravitational wave detector mirror suspensions.* Rev. Sci. Instr., **82** 011301

Husman M E, Torrie C I, Plissi M V, Robertson N A, Strain K A and Hough J 2000 *Modelling of multistage pendulums: triple pendulum suspension for GEO 600,* Rev. Sci. Instrum. **71** 2546-2551

Matichard F et al. 2010 *Prototyping, testing, and performance of the two-stage seismic isolation system for advanced LIGO gravitational wave detectors*, Proceedings of ASPE conference on Control of Precision Systems. 2010, 75-80.

Penn S D et al.., *Frequency and surface dependence of the mechanical loss in fused silica,* Phys. Lett. A, **352** 3-6, 2006

Plissi M V, Strain K A, Torrie C I, Robertson N A, Killbourn S, Rowan S, Twyford S M, Ward H, Skeldon K D and Hough J 1998, *Aspects of the suspension system for GEO 600.* Rev. Sci. Instr. **69** 3055-3061

Plissi M V, Torrie C I, Husman M E, Robertson N A, Strain K A, Ward H, Lück H, and Hough J 2000 *GEO 600 triple pendulum suspension system: seismic isolation and control* Sci. Instrum. **71** 2539-2545

Plissi M V et al. 2004 *An investigation of eddy-current damping of multi-stage pendulum suspensions for use in interferometric gravitational wave detectors.* Rev. Sci. Instrum., **75** 4516-4522

Raab F and Fine M 1997*The Effect of Earth Tides on LIGO Interferometers* LIGO document T970059
https://dcc.ligo.org/public/0028/T970059/000/T970059-01.pdf

Robertson N A et al. 2002 *Quadruple suspension design for Advanced LIGO,* Class. Quantum Grav. **19** 4043-4058

Rowan S, Twyford S M, Hough J ,Gwo D -H and Route R 1998 *Mechanical losses associated with the technique of hydroxide-catalysis bonding of fused silica.* Phys. Lett. A, **246** 471-478

Saulson P R 1990 *Thermal noise in mechanical experiments* Phys. Rev. D **42** 2437

Shapiro, 2011 *Fitting the Quad Noise Prototype Model to Measured Data*. LIGO Document T1000458
https://dcc.ligo.org/public/0013/T1000458/006/T1000458-v6.pdf

Shapiro B 2012 *Precision Control of a Quadruple Pendulum Test Mass Suspension for LIGO.* Proceedings of the American Society for Precision Engineering (ASPE) Spring Topical Meeting, Cambridge, MA. April 12, 2010, 69-74.

Sigg D and the LIGO Scientific Collaboration 2008, *Status of the LIGO detectors* Class. Quantum Grav. **25**,
114041

Strain K A and Shapiro B N 2012 *Damping and local control of mirror suspensions for laser interferometric gravitational wave detectors* Rev. Sci. Instrum. **83** 044501

Strain K 2006 *Electrostatic drive (ESD) results from GEO and application in Advanced LIGO* LIGO document T060015-00-K
https://dcc.ligo.org/public/0027/T060015/000/T060015-00.pdf

Tokmakov K V, Cumming A, Hough J,Jones R, Kumar R, Reid S, Rowan S, Lockerbie N A, Wanner A and Hammond G 2012 *A study of the fracture mechanisms in pristine silica fibres utilising high speed imaging techniques* Journal of Non-Crystalline Solids **358** 1699–1709

van Veggel A A et al. 2009., *Final Design Document ETM/ITM ears.* LIGO document T0900447
https://dcc.ligo.org/public/0005/T0900447/003/T0900447-v3_Final_design_document_ETM_ITM_ears.pdf

van Veggel M, Armandula H, Beveridge N , Cunningham W, Jones R and Moreno G 2012, *Preparation of an end or input test mass (ETM/ITM) (Hydroxide-Catalysis Bonding of ears)* LIGO document E1000278-v6
https://dcc.ligo.org/public/0010/E1000278/006/E1000278%20-%20Preparation%20of%20an%20end%20or%20input%20test%20mass%20%28ETMITM%29.pdf

Weiss R 2009, *Various Reports of Experiments Conducted on the Barkhausen Noise Research* LIGO document T080355
https://dcc.ligo.org/public/0001/T080355/001/T080355-v1.pdf